

## Article

# Geochronology and Geochemistry of the Granite Porphyry from the Qinglingou Gold Deposit, South Qinling, China: Implication for Petrogenesis and Mineralization

Kun Ding <sup>1,2</sup>, Xiuqing Yang <sup>2,\*</sup>, Hui Wang <sup>2</sup>, Ying Li <sup>3</sup>, Kai Liu <sup>4</sup>, Zhihui Wang <sup>1</sup>, Liang Zhao <sup>4</sup> and Yanjun Chen <sup>1</sup>

<sup>1</sup> Shaanxi Railway Institute, Weinan 714099, China; dingkun199008@163.com (K.D.); wzh\_kj@163.com (Z.W.); styjyzdxx@163.com (Y.C.)

<sup>2</sup> School of Earth Science and Recourses, Chang'an University, Xi'an 710054, China; wanghui16@chd.edu.cn

<sup>3</sup> Exploration and Development Research Institute of Changqing Oilfield Company, PetroChina, Xi'an 710018, China; liying2\_cq@petrochina.com.cn

<sup>4</sup> No. 713 Geological Team, Northwest Bureau of Geological Exploration for Nonferrous Metals, Shangluo 726000, China; 713dxy@163.com (K.L.); 2017027013@chd.edu.cn (L.Z.)

\* Correspondence: xiuqing2008@126.com

**Abstract:** The Zhashui-Shanyang ore cluster area is one of the most important gold polymetallic ones in northwestern China. The Qinglingou gold deposit is a newly discovered small-scale deposit in the Zhashui-Shanyang area. Gold mineralization closely related to acid intrusive rocks has been found for the first time in this area. In this paper, the geochronology, whole-rock geochemistry, and isotope signature of the granite porphyries in the deposit are studied. They are characterized by variable medium SiO<sub>2</sub> (67.22–71.72 wt.%), high K<sub>2</sub>O + Na<sub>2</sub>O contents (6.54–10.34 wt.%), and variable Al<sub>2</sub>O<sub>3</sub> (14.47–15.10 wt.%) values. The A/CNK ratios range from 0.90 to 1.23, and the A/NK ratios vary from 1.14 to 1.48. These rocks also contain biotite and amphiboles and are similar to peraluminous and high-K calc-alkaline I-type granites. The Qinglingou granite porphyries show relative enrichment of Rb, Th, and K, and depletion of Nb, Ta, P, Ti, and other high field strength elements. These porphyries are enriched in light rare earth elements relative to heavy rare earth elements with weak negative Eu anomalies ( $\delta\text{Eu} = 0.63\text{--}0.89$ ), which is interpreted to be the best age of crystallization of the Qinglingou porphyries. LA-ICPMS zircon U–Pb dating yields an age of  $211 \pm 1.2$  Ma ( $n = 16$ , MSWD = 0.39). The close spatial relationship between the ore bodies and granite porphyry dikes indicates that this age may represent the metallogenic age in this area. The zircons have <sup>176</sup>Hf/<sup>177</sup>Hf ratios ranging from 0.282625 to 0.282702, the  $\epsilon_{\text{Hf}}(t)$  values are near 0 and the two-stage zircon Hf model ages range from 1121 to 1296 Ma. These data indicate that the Qinglingou granite porphyries were derived from the interplay between mantle- and crustal-derived magmas. We therefore propose that there is potential gold in carbonate rocks at the periphery of porphyry-skarn copper-molybdenum deposits.

**Keywords:** geochemistry; zircon U–Pb dating; Qinglingou granite porphyry; Zhashui-Shanyang area; South Qinling Belt



**Citation:** Ding, K.; Yang, X.; Wang, H.; Li, Y.; Liu, K.; Wang, Z.; Zhao, L.; Chen, Y. Geochronology and Geochemistry of the Granite Porphyry from the Qinglingou Gold Deposit, South Qinling, China: Implication for Petrogenesis and Mineralization. *Minerals* **2022**, *12*, 707. <https://doi.org/10.3390/min12060707>

Academic Editors: Kunfeng Qiu, Callum Hetherington and Manuel Francisco Pereira

Received: 13 March 2022

Accepted: 30 May 2022

Published: 31 May 2022

**Publisher's Note:** MDPI stays neutral with regard to jurisdictional claims in published maps and institutional affiliations.



**Copyright:** © 2022 by the authors. Licensee MDPI, Basel, Switzerland. This article is an open access article distributed under the terms and conditions of the Creative Commons Attribution (CC BY) license (<https://creativecommons.org/licenses/by/4.0/>).

## 1. Introduction

The Qinling Orogen is characterized by multiple episodes of subduction, accretion, and collision between the North China Block (NCB) and South China blocks (SCB). It links the Dabie Mountains to the east and the Qilian and Kunlun Mountains to the west (Figure 1). Accompanying the intracontinental orogeny, the Neoproterozoic, Paleozoic, and Mesozoic tectono-magmatic events occurred in the Qinling Orogen, which hosts numerous deposits of different metals, in particular large Cu–Au–Pb–Zn–Mo deposits [1–3]. The South Qinling Belt is a significant Cu–Au polymetallic metallogenic belt and hosts abundant mineral resources, including world-class Au deposits. The Zhashui–Shanyang ore district, one of the most representative polymetallic ore clusters within the northern segment of this orogen,

hosts 20 gold deposits with different Au ore reserves, such as Ertaizi, Qinglingou, Xiajiadian, Wangjiaping, and etc. The influence of multi-stage tectonic magmatic events in the Qinling orogenic belt led to the Cu and Au polymetallic mineralization. These mineralizations were closely related to Triassic, Late Jurassic, and Early Cretaceous magmatic events that have been strongly developed in the area [4,5].

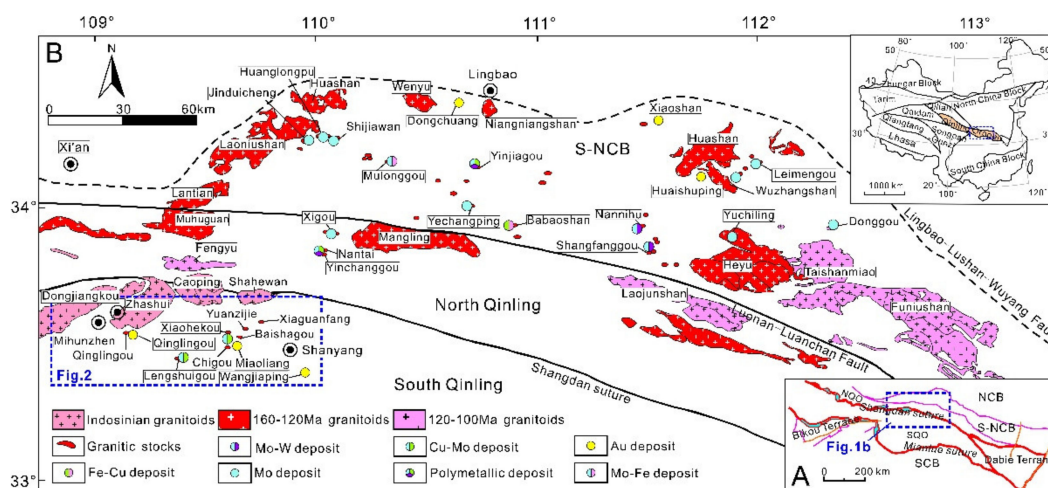


**Figure 1.** Sketch map showing the location and major tectonic units of the Qinling Orogen, central China (A); Geological map of the Qinling Orogen, showing the distribution of the Mesozoic granitoids and major deposits (B) [2].

Previous studies mainly focused on petrology, geochemistry, and geochronology [3–19]. The results have shown the existence of SEDEX-type deposits and medium-scale, porphyry-skarn Cu (Mo) and Carlin-type Au deposits, with examples including the Daxigou Fe deposit, Yindongzi Ag–Pb deposit, Mujiazhuang Cu deposit, Xiaohekou, Chigou and Lengshuigou Cu (Mo) deposits, and Ertaizi Au deposit. The intensive Indosinian (e.g., the Dongjiangkou, Zhashui, Shahewan, and Caoping pluton) and Yanshanian (e.g., the Lengshuigou, Chigou, Baishagou, and Shuangyungou pluton) magmatic activity resulted in the emplacement of a number of some granitoids, accompanied by a variety of mineralization [14,17–19]. Several hydrothermal porphyry-skarn Cu, Mo, Au, and Fe deposits or occurrences were discovered within hypabyssal intrusions, such as the Xiaohekou, Lengshuigou, and Chigou [7,9]. However, little has been reported on the comprehensive understanding of the tectonic magmatic evolution and mineralization of the district.

The intrusive rocks in the Qinglingou mining district are granite porphyry and lamprophyre dikes. Granite porphyries, located in the northwest Zhashui-Shanyang district, are widespread in the Qinglingou gold deposit. The timing and magmatic evolution of these plutons and associated deposits, as well as their potential for future mineral exploration, remain equivocal.

With this in mind, in this study, we present the whole-rock geochemistry and in situ zircon U–Pb–Hf isotope signature for the Qinglingou granite porphyries from the Zhashui-Shanyang district to (1) constrain the timing of the granite emplacement; (2) understand the magma source, petrogenesis, and metallogenic implications; and (3) evaluate future exploration potential.

## 2. Geological Setting

The Zhashui-Shanyang, located in the western part of the South Qinling Belt (Figure 1B), is abundant in the Indosinian-Yanshanian granitoids and Au and Cu–Mo polymetallic deposits. The multiple Jurassic to Cretaceous porphyry-skarn Cu (Mo) orebodies were discovered in the Zhashui-Shanyang district in the southern Qinling Orogen within or near the Late Jurassic–Early Cretaceous granitic intrusions, such as Xiaohekou, Chigou and

Lengshuigou Cu (Mo) deposits. The area was divided into two gold ore belts along the Shanyang-Fengzhen Fault. The two belts are the southern margin of the Ertaizi-Fengzhen-Xiajiadian Carlin and Carlin-like type gold belt and Qinglingou-Wangjiagou-Miaoliang Carlin and Carlin-like type gold belt, both of which extend from north to south (Figure 2). The Zhashui-Shanyang area mainly comprises Devonian and Carboniferous quartz sandstone, siltstone, slate, and limestone. The Zhashui-Shanyang area is an important part of the Qinling orogenic belt. The area is bounded by the NWW-trending Shangxian-Danfeng Fault to the north, and the NW-trending Fengzhen-Shanyang Fault to the south. The Shanyang-Fengzhen and Zhen'an-Banyanzhen regional fault zones run through the whole area, controlling the distribution of the main orebody in the area. The structural intersection part is composed of multi-stage EW and NNE, NNW fault. What is more, the SN fault (or NNE fault) has also developed widely in the ore concentration area. These faults are also the main location of deposits, which are conducive to the upward migration of ore fluid. The magmatic activity in the Zhashui-Shanyang area is relatively intensive and is characterized by multi-period and multi-stage. Indosinian to Yanshanian was a significant period of magmatism in the Zhashui-Shanyang area. The Indosinian granitoids were mainly located in the West and North of the area, such as Dongjiangkou, Zhashui, Shahewan, and Caoping pluton with large exposure areas which are mainly spatially and temporally associated with Cu, Au, Mo, Pb, Zn and Fe mineralization, and others.

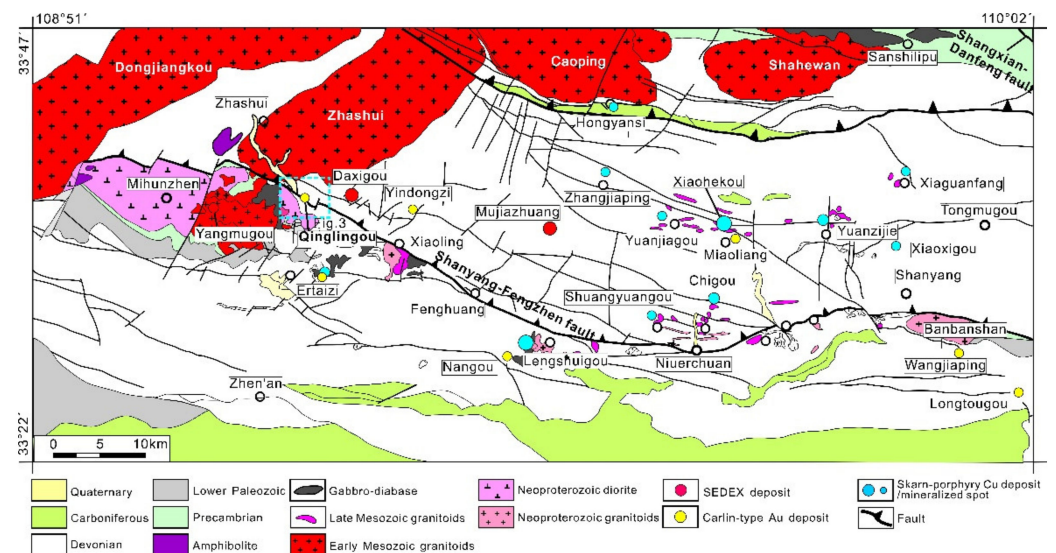


**Figure 2.** Geological map of the Zhashui-Shanyang ore district cluster showing the distribution of granitoids and deposits [20].

The Yanshanian granitoid intrusions were distributed along both sides of the Fengzhen-Shanyang Fault and occurred as small-scale dikes. They are mainly distributed in the east and middle of the area, such as Miaoliang, Lengshuigou, Xiaohekou, Chigou, Baishagou plutons, etc. The Yanshanian granitoid intrusions mainly host two different types of deposits, such as porphyry type deposit and skarn type deposit [17,21–26].

The Qinglingou gold deposit is located in the northwest of Zhashui-Shanyang area ( $109^{\circ}10' E$ ,  $33^{\circ}38' N$ ) (Figure 3). The rocks exposed in this ore district are mainly Middle Devonian sedimentary units belonging to the Niuerchuan Group. A few scattered felsic magmatic dikes (mainly granite porphyries) intrude into the Niuerchuan Group. The major fault of this ore district is the Shanyang-Fengzhen Fault, controlling the ore-forming process of Au and accompanying several NNW- and NNE-trending secondary faults. There are eleven main orebodies with a grade of  $0.75 \times 10^{-6}$  to  $6.2 \times 10^{-6}$  Au within the Qinglingou deposit, which developed in both carbonate rocks and granite porphyry dikes, as well as host-rock sedimentary units. The orebodies are usually stratigraphically controlled and show stratabound, lenticular, and vein-like shapes. Granite porphyry dikes near the ore

show pyritization and silicification. The geological characteristics of the Qinglingou gold deposit are close to those of the Carlin-type gold deposit, and the geochemical composition of the deposit is similar to that of the Yangshan Carlin-type gold deposit.

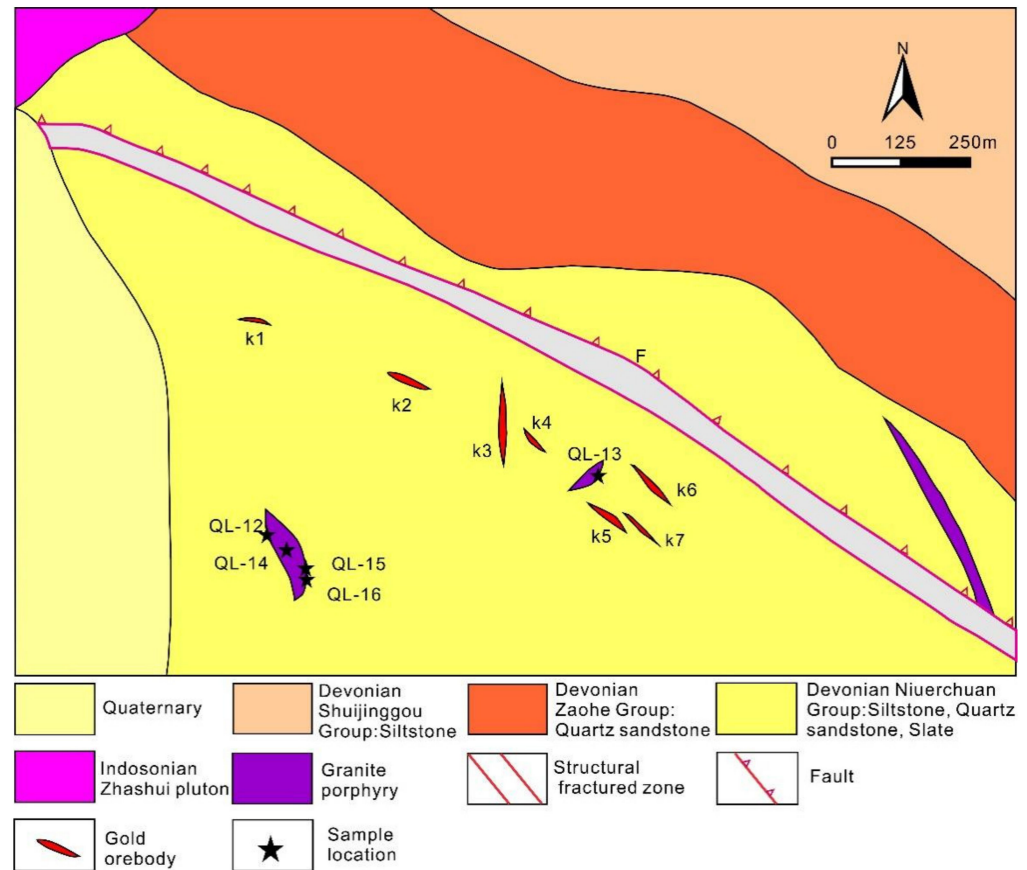


**Figure 3.** Geological map of the Qinglingou area in the Zhashui-Shanyang ore district cluster (Modified after No. 713 Geological Team, Northwest Bureau of Geological Exploration for Nonferrous Metals).

According to the mineral assemblages and cross-cutting relationships of veinlets, three stages of mineralization can be identified from early to late. The first is the quartz-pyrite stage, during which the quartz is milky to gray in color with small particle sizes. Pyrite is present as euhedral to subhedral crystals with disseminated, veinlet, and irregular massive forms. The second is the quartz-multimetal sulfide stage, actually the main mineralization stage, during which ore-related alteration includes sulfidization (arsenopyrite and pyrite), sericitization, silicification, and carbonatization. The third is the quartz, and carbonate stage, during which carbonate veinlets have in-filled open-space fissures and cross-cut the earlier veins. There are a large number of pyrite, arsenopyrite, pyrrhotite, and chalcopyrite, of which pyrite is the main gold-bearing mineral in the Qinglingou gold deposit. The gangue minerals include quartz, biotite, dolomite, sericite, feldspar, and epidote, with accessory zircon, and monazite (Figure 4).

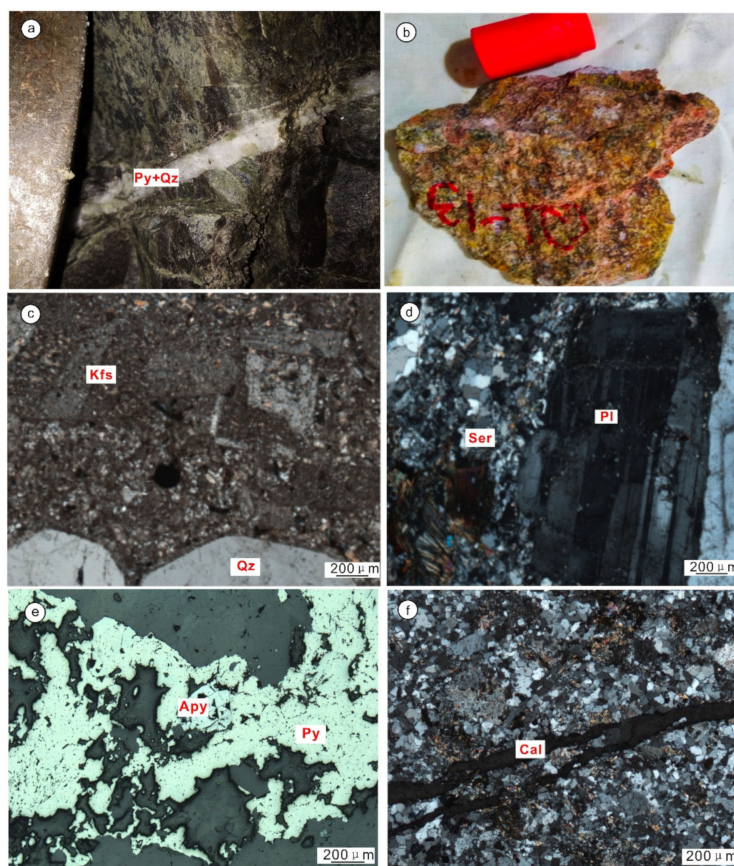


**Figure 4.** Representative field and microscopic photographs of the Qinglingou Au deposit; scale for (a) Quartz–pyrite vein in the mining district; (b) Granodiorite porphyry sample from the pit; (c,d) Phenocrysts are K–feldspar, plagioclase and quartz, and the matrix is quartz and sericite; (e) Arsenopyrite and pyrite vein stage; (f) Calcite vein stage. Apy–arsenopyrite; Cal–calcite; Pl–plagioclase; Kfs–Potassic feldspar; Qz–quartz; Ser–sericite; Py–pyrite.

### 3. Samples and Analytical Methods

#### 3.1. Sample Description

The collected samples in this study showed no signs of weathering, intense hydrothermal alteration, or superimposed mineralization. One sample (QL-13) was taken from the Qinglingou pluton for zircon U–Pb dating, and further chosen for zircon Hf isotopic analysis. In total, five samples of granite porphyry were taken for whole-rock geochemical analyses. The petrographical characteristics of these samples are described as follows:

The Qinglingou dikes are pink-gray to white in color with a porphyritic texture. The phenocrysts of sample QL-13 granite porphyry mainly consist of 5%–10% quartz (0.25–0.45 mm), 10% plagioclase (0.05–0.15 mm), and 10%–15% K-feldspar (0.05–0.30 mm), <5% biotite. Besides, hornblende is also observed. Quartz occurs as subhedral-anhedral grains, with small particle sizes. K-feldspar mainly occurs as a subhedral granular microcline with well-developed crosshatched twinning. Plagioclase is present as euhedral to subhedral oligoclase with polysynthetic twinning. The matrix minerals are made up of quartz (10%–20%), plagioclase (25%–35%), K-feldspar (15%–20%), and biotite (<5%). The accessory minerals are apatite and zircon. The other samples show typical porphyritic texture and consist mainly of coarse-grained quartz (0.15–0.75 mm), plagioclase (0.5–1.25 mm) and K-feldspar (0.05–0.55 mm) phenocrysts, together with fine-grained felsic minerals in the matrix surrounding the phenocrysts (Figure 4b–d).

### 3.2. Major and Trace Element Analysis

The fresh portions of samples were powdered to 200 mesh and then dried for analysis. Major and trace elements were carried out at the Mineralization and Dynamics Laboratory of the Ministry of Land and Resources, Chang'an University, Xi'an, China. Major elements were determined on flux glass discs by XRF with analytical precision generally better than 5%. Trace elements, including rare earth elements, were determined using ICP-MS (Agilent 7500a). A set of USGS and Chinese national rock standards include AGV-2, AMH-1 and GBPG-1. The accuracy for all trace elements is mostly between 1% and 5% [24].

### 3.3. Zircon U-Pb Dating

The representative samples QL-13 were selected for in situ zircon U-Pb, trace elements, and Lu-Hf isotope analyses. These analyses were conducted at the Mineralization and Dynamics Laboratory of the Ministry of Land and Resources, Chang'an University, Xi'an, China.

Sample QL-13 was sieved for separating zircon grains using conventional heavy liquid and magnetic techniques at the Langfang Tuoxuan rock mine Testing Service Co., Ltd., China. Representative zircons were handpicked under a binocular microscope. Then zircon grains were mounted in epoxy. The polished mounts were imaged under cathodoluminescence (CL). Zircon U-Pb ages and trace elements were obtained using an Analyte Excite 193 nm Laser Ablation coupled to an Agilent 7700E ICP-MS. The diameter of the laser ablation crater was 32  $\mu\text{m}$ . The detailed operating conditions and analytical methods are based on Liu et al. [27]. The U-Pb age was calculated using Isoplot 3.7 software [28]. The results were achieved by repeated analyses in accordance with the zircon standards 91500 and GJ-1, with a precision of the U-Pb ages of 1%.

### 3.4. Zircon Lu-Hf Analysis

In-situ Lu-Hf analysis for zircons was carried out using a Nu PlasmaHR MC-ICPMS Laboratory of Beijing Kehui Testing Technology Co., Ltd., Beijing, China. Details of instrumental conditions and data acquisition were described by Yuan et al. [29]. The measurements were conducted on the same zircon grains previously analyzed for U-Pb isotopes with a 43  $\mu\text{m}$  ablation spot size. The laser repetition rate was 5 Hz. Calculations of zircon isotope ratios were performed by ICP-MS DataCal [29]. Harvard 91500 and GJ-1 were used as reference standards during analyses. The primary reference material for Hf isotope measurement used for monitoring accuracy and precision of internally corrected Hf isotope ratios was zircon 91500 and Mudtank.

## 4. Results

### 4.1. Whole-Rock Geochemistry

The major and trace element compositions of samples from the Qinglingou plutons are listed in Table 1.

The major element compositions show only a slight variation, with medium  $\text{SiO}_2$  (67.22–71.72 wt.%, average of 69.34 wt.%) and  $\text{Al}_2\text{O}_3$  (14.47–15.10 wt.%, average of 14.9 wt.%), high  $\text{K}_2\text{O}$  (3.53–4.63 wt.%, average of 4.20 wt.%), but low  $\text{P}_2\text{O}_5$  (0.08–0.14 wt.%, average of 0.11 wt.%) contents. The Qinglingou, Zhashui, Caoping, and Shahewan plutons, are all classified as the quartz monzonite, granodiorite, and granite series in the total  $\text{Na}_2\text{O} + \text{K}_2\text{O}$  vs.  $\text{SiO}_2$  diagram (TAS; Figure 5a). They mainly belong to the high-K calc-alkaline series in the  $\text{K}_2\text{O}$  vs.  $\text{SiO}_2$  diagram (Figure 5b). Figure 5c shows that the Shahewan plutons and Zhashui plutons display the quasi-aluminous series, and the Qinglingou granite porphyry and Caoping plutons are typical metaluminous to weakly peraluminous ( $A/\text{CNK} = 0.90\text{--}1.23$ , an average of 1.05, less than 1.1;  $A/\text{NK} = 1.14\text{--}1.48$ , an average of 1.30), indicating peraluminous and high-K calc-alkaline I-type characteristic, similar to the previous results in the Zhashui-Shanyang area [11,19].

**Table 1.** Major (wt.%) and trace elements(ppm) of the granite porphyries from the Qinglingou gold deposit.

Analysis	QL-12	QL-13	QL-14	QL-15	QL-16
SiO <sub>2</sub>	71.72	69.1	69.23	69.45	67.22
TiO <sub>2</sub>	0.33	0.44	0.39	0.42	0.45
Al <sub>2</sub> O <sub>3</sub>	14.47	14.97	14.93	15.1	15.05
TFe <sub>2</sub> O <sub>3</sub>	2.03	2.79	2.62	1.2	2.64
MnO	0.02	0.05	0.03	0.02	0.05
MgO	0.73	1.02	0.68	0.1	0.55
CaO	1.04	0.88	0.78	2.01	2.85
Na <sub>2</sub> O	3.01	4.17	4.9	5.71	3.73
K <sub>2</sub> O	4.59	4.63	4.53	3.53	3.74
P <sub>2</sub> O <sub>5</sub>	0.1	0.14	0.08	0.09	0.14
LOI	1.29	1.46	1.05	2.01	3.42
TOTAL	99.33	99.65	99.22	99.64	99.84
A/NK	1.459	1.261	1.152	1.143	1.478
A/CNK	1.225	1.111	1.038	0.895	0.979
Rb	80.10	83.79	39.43	41.84	87.11
Ba	859	913	1180	650	958
Th	19.38	15.66	9.44	11.93	17.59
U	4.93	3.53	1.12	0.95	3.55
K	38,087	38,419	37,589	29,291	31,034
Ta	1.37	1.42	1.29	1.66	1.45
Nb	12.92	14.23	19.43	21.83	14.22
La	21.01	23.28	40.79	29.87	26.01
Ce	33.75	41.12	73.71	54.61	45.25
Sr	275.92	214.53	98.54	149.60	264.58
Nd	13.28	15.92	29.74	20.68	18.09
P	436.62	611.27	349.30	392.96	611.27
Zr	121.99	164.18	343.34	368.04	159.51
Hf	3.43	4.28	7.18	7.64	4.16
Sm	2.13	2.85	5.02	3.59	3.37
Ti	1980	2640	2340	2520	2700
Y	7.84	10.56	20.96	18.75	12.64
Yb	0.88	1.07	2.04	1.91	1.20
Lu	0.13	0.15	0.28	0.29	0.19
ΣREE	80.36	95.82	173.03	127.94	107.46
LREE	74.62	88.57	158.98	115.53	98.74
HREE	5.74	7.25	14.05	12.40	8.73
LREE/HREE	13.01	12.22	11.31	9.32	11.32
La <sub>N</sub> /Yb <sub>N</sub>	17.09	15.66	14.37	11.20	15.54
δEu	0.83	0.89	0.65	0.63	0.79

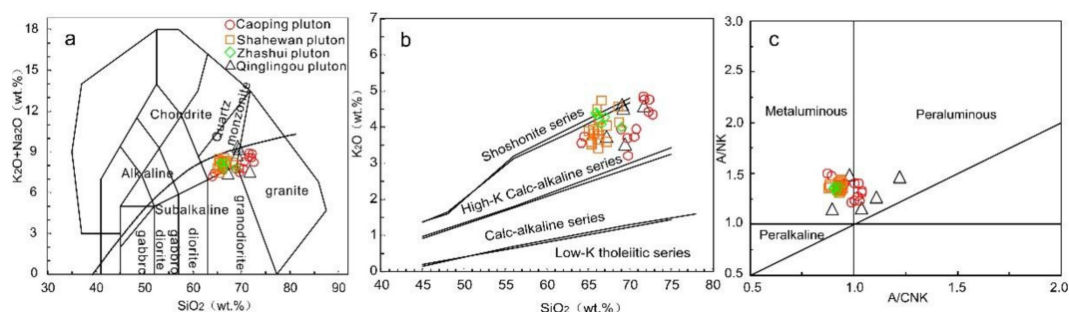


**Figure 5.** (a) Plots of Na<sub>2</sub>O + K<sub>2</sub>O vs. SiO<sub>2</sub> [30], (b) K<sub>2</sub>O vs. SiO<sub>2</sub> [31], and (c) A/NK [molar ratio Al<sub>2</sub>O<sub>3</sub>/(Na<sub>2</sub>O + K<sub>2</sub>O)] vs. A/CNK [molar ratio Al<sub>2</sub>O<sub>3</sub>/(CaO + Na<sub>2</sub>O + K<sub>2</sub>O)] [32]; Granitoid data of the Zhashui-Shanyang district are from [11,19].

All samples have similar REE patterns characterized by right-inclined on the chondrite-normalized rare earth element (REE) diagram (Figure 6a) and relatively low ΣREE

(80.37–173.04 ppm), enriched in light rare earth elements (LREEs) with flat HREE patterns (HREEs)  $[(La/Yb)_N = 11.20–17.09]$ . Most of the granite porphyries display weakly negative Eu anomalies ( $\delta Eu = 0.63–0.89$ ). On the primitive mantle-normalized trace element spidergram (Figure 6b), most of the Qinglingou granite porphyry show pronounced relative enrichment of large ion lithophile elements (LILEs; e.g., Rb, Th, and K), and depleted in high field strength elements (HFSEs; e.g., Nb, Ta, and Ti) and P.

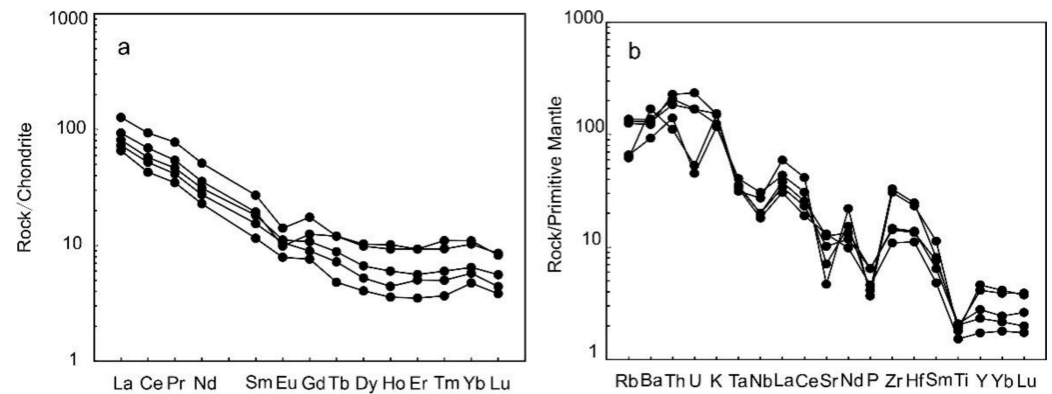


**Figure 6.** (a) Chondrite-normalized REE patterns and (b) primitive mantle (PM) normalized trace elements diagrams of the granite porphyry from Qinglingou. The values of chondrite and PM are from [33,34].

#### 4.2. Zircon U-Pb Ages

The analytical results of LA-ICPMS zircon U-Pb dating are presented in Table 2. The representative CL images of the dated zircons and Concordia diagrams are shown in Figure 7a. Zircon grains from the sample QL-13 are prismatic and 150–200  $\mu\text{m}$  long with length/width ratios of 1:1–2:1. Most zircons display dark gray CL images and recognizable clear oscillatory zoning, indicating a magmatic origin for the zircons. All zircons have Th and U concentrations of 248–1026 and 292–1093 ppm, respectively, and the Th/U ratios range from 0.106 to 2.003. All 16 zircons from sample QL-13 yielded a weighted U–Pb zircon age of  $211 \pm 1.2$  Ma (MSWD = 0.39) (Figure 7b).

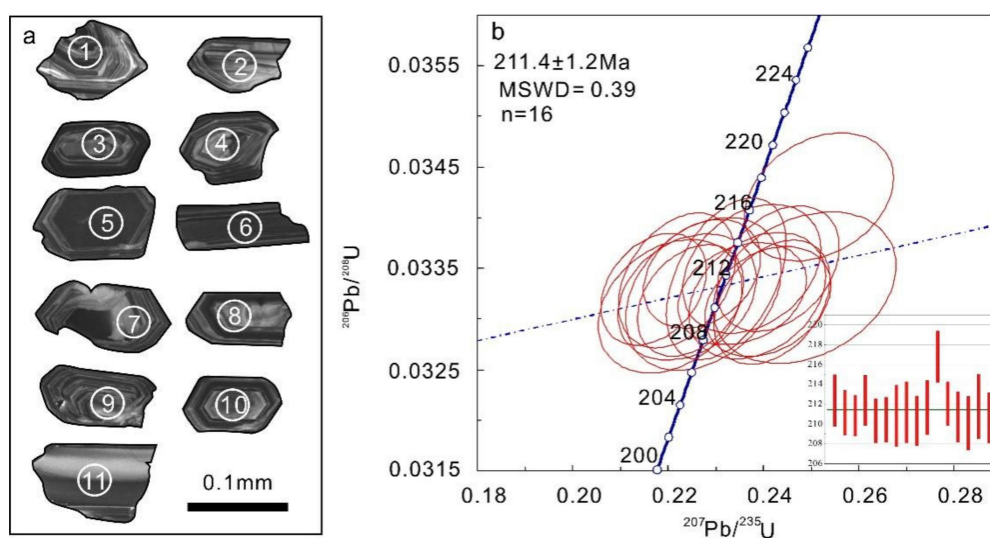


**Figure 7.** (a) Cathodoluminescence images, and (b) LA-ICPMS zircon U-Pb Concordia diagrams of ore-related granite porphyry from the Qinglingou deposit.

**Table 2.** LA-ICPMS U-Pb zircon isotope ratios of the granite porphyry from the Qinglingou Au deposit.

Analysis	Concentration (ppm)			Isotopic Ratio						Isotopic Ages (Ma)						Con.	
	Pb	Th	U	Th/U	<sup>207</sup> Pb/ <sup>206</sup> Pb	1σ	<sup>207</sup> Pb/ <sup>235</sup> U	1σ	<sup>206</sup> Pb/ <sup>238</sup> U	1σ	<sup>207</sup> Pb/ <sup>206</sup> Pb	1σ	<sup>207</sup> Pb/ <sup>235</sup> U	1σ	<sup>206</sup> Pb/ <sup>238</sup> U		1σ
<b>QL-13-Granodiorite</b>																	
QL-13-1	28.78	520	743	0.70	0.0513	0.0020	0.2375	0.0096	0.0335	0.0004	254	89	216	8	212	3	98%
QL-13-4	31.8	680	780	0.87	0.0473	0.0016	0.2170	0.0073	0.0333	0.0004	64.9	77.8	199	6	211	2	94%
QL-13-5	23.15	293	645	0.45	0.0513	0.0019	0.2355	0.0089	0.0332	0.0003	257	85	215	7	211	2	98%
QL-13-7	27.81	503	715	0.70	0.0525	0.0017	0.2431	0.0085	0.0335	0.0004	306	81	221	7	212	3	96%
QL-13-9	31.8	688	800	0.86	0.0526	0.0019	0.2409	0.0087	0.0332	0.0004	322	81	219	7	210	2	95%
QL-13-10	37.8	794	936	0.85	0.0491	0.0016	0.2247	0.0073	0.0332	0.0004	150	81	206	6	210	2	97%
QL-13-11	11.72	248	292	0.85	0.0499	0.0024	0.2274	0.0108	0.0332	0.0005	191	111	208	9	211	3	98%
QL-13-12	13.59	314	334	0.94	0.0542	0.0027	0.2487	0.0127	0.0333	0.0005	389	113	225	10	211	3	93%
QL-13-13	34.1	875	810	1.08	0.0527	0.0016	0.2418	0.0080	0.0332	0.0004	322	70	220	7	210	3	95%
QL-13-14	28.9	633	702	0.90	0.0483	0.0018	0.2219	0.0081	0.0334	0.0004	122	82	203	7	212	3	96%
QL-13-16	44.0	795	1093	0.73	0.0534	0.0022	0.2517	0.0103	0.0342	0.0004	343	90	228	8	217	3	95%
QL-13-17	38.5	757	975	0.78	0.0493	0.0017	0.2271	0.0081	0.0334	0.0004	161	83	208	7	212	2	97%
QL-13-18	19.38	311	510	0.61	0.0520	0.0020	0.2387	0.0095	0.0332	0.0004	287	87	217	8	211	3	96%
QL-13-19	17.53	379	439	0.86	0.0484	0.0022	0.2204	0.0100	0.0331	0.0004	120	112	202	8	210	3	96%
QL-13-20	33.4	1026	746	1.37	0.0505	0.0017	0.2322	0.0083	0.0334	0.0005	217	47	212	7	212	3	99%
QL-13-21	26.7	816	602	1.35	0.0488	0.0020	0.2240	0.0096	0.0332	0.0004	139	98	205	8	211	3	97%

4.3. Zircon Lu-Hf Isotope Analysis

The results of in situ Hf isotope analysis for the zircon grains from sample QL-13 are listed in Table 3. Most zircons have low  $^{176}\text{Lu}/^{177}\text{Hf}$  ratios, ranging from 0.000825 to 0.002327 (all are less than 0.002), which indicate little radioactive Hf accumulation after the emplacement of the rock mass, except zircon QL13-11, which provided slightly positive  $^{176}\text{Lu}/^{177}\text{Hf}$  values of 0.002327. The zircon  $^{176}\text{Hf}/^{177}\text{Hf}$  ratio can, therefore, be used to explore the genetic information on petrogenesis [35,36]. Sixteen representative magmatic zircons from the Qinglingou granite porphyry sample were analyzed in this study. The initial  $^{176}\text{Hf}/^{177}\text{Hf}$  ratios vary from 0.282625 to 0.282702 (average of 0.282615), and  $\epsilon_{\text{Hf}}(t)$  values range from  $-0.77$  to  $1.98$  (average of  $0.41$ ), similar to the  $\epsilon_{\text{Hf}}(t)$  values of Zhashui plutons, Caoping plutons and Shahewan plutons in the Zhashui-Shanyang area (Figure 8). These zircons show relatively consistent one-stage Hf model ages ( $T_{\text{DM1}}$ ) varying from 786 to 1296 Ma (average of 851 Ma), with two-stage model ages ( $T_{\text{DM2}}$ ) of 1121–1296 Ma (average of 1222 Ma).

Table 3. Zircon Lu-Hf isotopic compositions of the granite porphyry from the Qinglingou Au deposit.

Analysis	Isotopic Ages (Ma)	$^{176}\text{Yb}/^{177}\text{Hf}$	$^{176}\text{Lu}/^{177}\text{Hf}$	$^{176}\text{Hf}/^{177}\text{Hf}$	$2\sigma$	$\epsilon_{\text{Hf}}(0)$	$\epsilon_{\text{Hf}}(t)$	$T_{\text{DM1}}$	$T_{\text{DM2}}$	$f_{\text{Lu/Hf}}$
QL13-1	212	0.024375	0.001045	0.282625	0.000017	-5.19	-0.68	0.888	1.292	-0.969
QL13-2	211	0.032541	0.001431	0.282651	0.000016	-4.26	0.17	0.860	1.237	-0.957
QL13-3	211	0.038204	0.001682	0.282664	0.000017	-3.82	0.58	0.848	1.211	-0.949
QL13-4	212	0.017897	0.000825	0.282639	0.000015	-4.70	-0.16	0.864	1.259	-0.975
QL13-5	210	0.030478	0.001479	0.282672	0.000016	-3.55	0.86	0.833	1.192	-0.955
QL13-6	210	0.036056	0.001644	0.282628	0.000017	-5.10	-0.72	0.899	1.293	-0.950
QL13-7	211	0.032284	0.001342	0.282702	0.000018	-2.46	1.98	0.786	1.121	-0.960
QL13-8	211	0.033053	0.001413	0.282660	0.000014	-3.97	0.46	0.848	1.218	-0.957
QL13-9	210	0.034023	0.001498	0.282626	0.000015	-5.17	-0.77	0.898	1.296	-0.955
QL13-10	212	0.030665	0.001302	0.282657	0.000016	-4.06	0.42	0.849	1.222	-0.961
QL13-11	217	0.055593	0.002327	0.282687	0.000016	-3.02	1.42	0.830	1.162	-0.930
QL13-12	212	0.031281	0.001443	0.282696	0.000014	-2.69	1.77	0.797	1.136	-0.957
QL13-13	211	0.022025	0.000984	0.282644	0.000014	-4.52	-0.02	0.860	1.249	-0.970
QL13-14	210	0.031548	0.001382	0.282656	0.000017	-4.10	0.33	0.852	1.226	-0.958
QL13-15	212	0.037395	0.001636	0.282661	0.000014	-3.93	0.49	0.852	1.217	-0.951
QL13-16	211	0.025462	0.001138	0.282657	0.000013	-4.06	0.41	0.846	1.222	-0.966

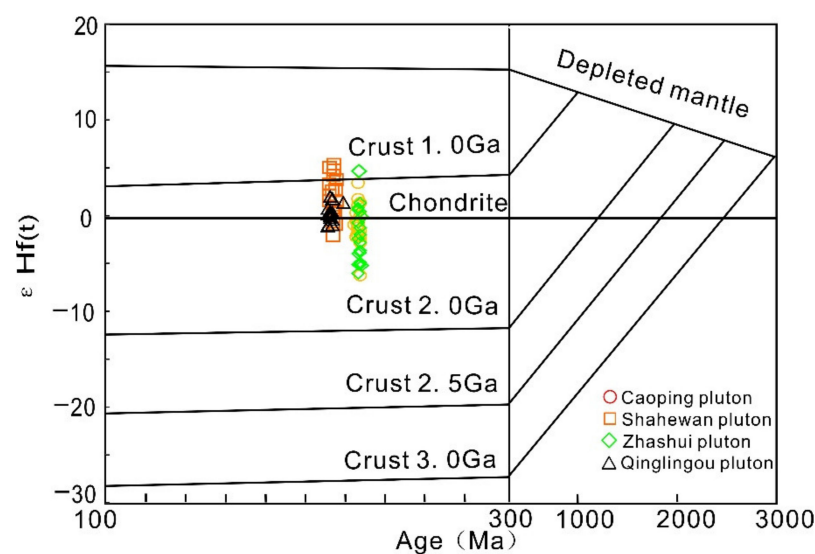
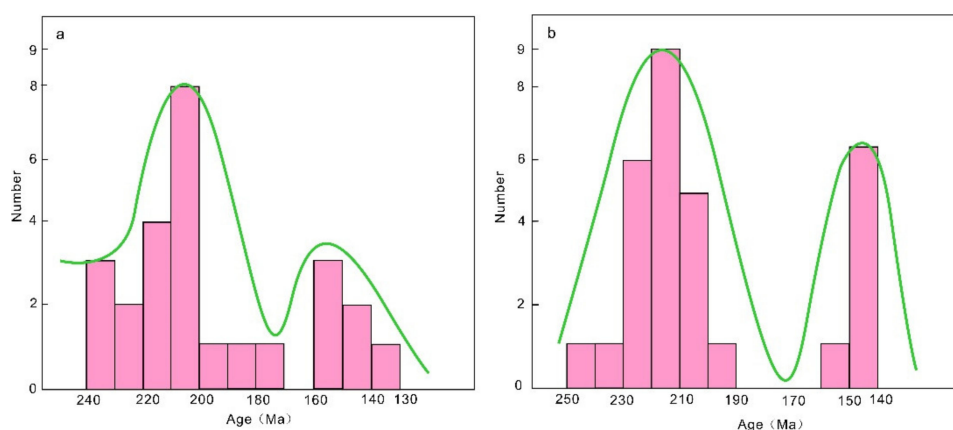


Figure 8. Plot of zircon  $\epsilon_{\text{Hf}}(t)$  values vs. crystallization ages for the granite porphyry from the Qinglingou Au deposit. Other granitoid data in the Zhashui-Shanyang district are from [11,19].

## 5. Discussion

### 5.1. Formation Age

There are two important gold deposit metallogenic events between the Indosinian and Yanshanian periods in the Qinling orogenic belt (Figure 9; Table 4). For example, Liba, Chaima, Simaoling, Zaozigou, Manaoke, Jinlongshan, Huaishuping, and Shanggong gold deposits were formed during Indosinian period, with the metallogenic age varying from 233 Ma to 202 Ma. Yanshanian gold mineralization events have also occurred in the Qinling area, such as Xiaoshan, Dongchuang and Donggou gold deposits, and the metallogenic age is concentrated with a peak of 153–142 Ma [37–54]. In addition, both Indosinian and Yanshanian gold mineralization events have been identified in Zhaishang and Baguamiao gold deposits.



**Figure 9.** Histogram of metallogenic age of gold deposits in Qinling orogenic belt (See Table 4 for the detail) (a) [37–54], and intrusive age of Zhashui-Shanyang area (b) [6–13,20].

**Table 4.** Formation age of gold deposits in Qinling orogenic belt.

Belt	Deposit	Minerals	Method	Metallogenic Age (Ma)	Reference
West Qinling	Liba	Muscovite in Quartz	Ar-Ar	205.02 ± 3.53	[37]
		muscovite	Ar-Ar	215.6 ± 1.3	[38]
	Dugou	Pyrite and Quartz	Rb-Sr	171.6 ± 26.9	[39]
		Scheelite	Sm-Nd	222.6 ± 9.8	[40]
	Zhaishang	Calcite	Sm-Nd	144.1 ± 3.5	[41]
		Quartz inclusion	Rb-Sr	153 ± 20	[42]
	Maquan	Muscovite in Quartz	Ar-Ar	190.71 ± 2.37	[43]
	Yangshan	Muscovite in Quartz	Ar-Ar	232.58 ± 1.59	[42]
	Baguamiao	Muscovite in Quartz	Ar-Ar	131.9 ± 0.98	[42]
		Carbonate minerals	Sm-Nd	209.3 ± 4.2	[44]
	Chaima	Dolomite and Calcite	Sm-Nd	203.2 ± 1.6	[45]
	Simaoling	Sericite	Ar-Ar	211.9 ± 1.5	[46]
	Zaozigou	Monazite	U-Pb	211 ± 3	[47]
	Manaoke	Quartz inclusion	Rb-Sr	210 ± 35	[48]
	Jinmuda	Quartz inclusion	Rb-Sr	187 ± 12	[49]
Jinlongshan	Sericite	Ar-Ar	232.7 ± 6.9	[50]	
Donggou	Sericite	Ar-Ar	142	[51]	
East Qinling	Dongchuang	Pyrite	Re-Os	150 ± 21	[52]
	Dianfang	Garnet	Sm-Nd	204 ± 2	[53]
	Shanggong	Altered Sericite	Ar-Ar	236.4 ± 2.5	[53]
	Xiaoshan	Sericite	Ar-Ar	156 ± 1	[53]
	Huaishuping	Molybdenite	Re-Os	202.2 ± 8	[54]
	Yangmugou	Molybdenite	Re-Os	203.6 ± 8.7	Unpublished data

The Zhashui-Shanyang area is one of the most important metallogenic districts in the Qinling orogenic belt. The granitic magmatism in the Indosinian and Yanshanian periods in the area was intense (Table 5), which was accompanied by large-scale Cu and Au mineralization.

**Table 5.** Summary intrusion ages of Indosinian Yanshanian Pluton in Zhashui-Shanyang area.

Era	Pluton	Location	Lithology	Zircon LA-ICPMS U-Pb Age (Ma)	Reference	
Indosinian period	Dongjiangkou	Yingpanjie	Granodiorite	246.8 ± 2.5	[9]	
		Yingpanjie	Biotite monzogranite	222.6 ± 0.5	[10]	
		Yingpanjie	Biotite monzogranite	219–209	[8]	
		Yaowangtang	Tonalite	221 ± 2	[6]	
		Meizhuang	Granodiorite	220 ± 2	[6]	
		Shaluozhang	Tonalite	214 ± 2	[6]	
	Shahewa			Rapakivi granite	212 ± 0.93	[11]
				Rapakivi granite	209–205	[13]
	CaoPing			Monzonitic granite	224.1 ± 1.1	[9]
				Monzonitic granite	220.0 ± 2.0	[6]
	Zhashui	Xichuanjie		Biotite adamellite	213.6 ± 1.8	[12]
		Xichuanjie		Granite	233.6 ± 1.3	[9]
		—		Biotite adamellite	224.8 ± 1.1	[9]
Qinglingou			Granite porphyry	211.5 ± 2.9	This paper	
Liyuantang	—		Quartz monzonite	956.1 ± 4.5	[9]	
	—		Granite	203.6 ± 2.2	[9]	
Yanshanian period	Miaoliang		Diorite porphyrite	144.3 ± 0.7	[7]	
	Xiaguanfang		Granodiorite porphyry	142.7 ± 0.5	[7]	
	Xiaohekou		Diorite	150.2 ± 0.8	[7]	
	Chigou		Quartz diorite	146 ± 1	[20]	
	Lengshuigou		Granite porphyry	143.9 ± 0.7	[7]	
	Lengshuigou		Granodiorite porphyry	142.2 ± 0.5	[7]	
	Yuangjiagou		Monzonitic granite porphyry	144.5 ± 1.0	[7]	
	Tudigou		Monzonitic granite	144.6 ± 0.4	[7]	

The Yanshanian granitoids in the area are mainly hypabyssal-ultra hypabyssal intermediate and acid minor intrusions, such as Miaoliang, Lengshuigou, Yuanjiagou, Xiaohekou, Chigou, Yuanziji, Xiaguanfang, Tudigou, Mayingou, Shuangyuangou, and Baishagou plutons. The Cu, Mo, Fe, and Au deposits (occurrences) are mostly related to these Yanshanian plutons [5,25]. The single mineral Sm-Nd analysis of the Longtougou gold deposit yielded an age of 141 ± 3.6 Ma, similar to the dolomite Sm-Nd ages of 139.6 ± 0.98 Ma [25] and sericite <sup>40</sup>Ar/<sup>39</sup>Ar ages of 142 Ma [51]. Geochronological studies strongly imply that Yanshanian intrusive and metallogenic events occurred in the area.

The Zhashui plutons, which are located in the north of Qinglingou plutons, yield zircon LA-ICPMS U-Pb ages of 234–213 Ma. However, the new zircon LA-ICPMS U-Pb analysis of the Qinglingou granite porphyry in the study yielded a weighted mean <sup>206</sup>Pb/<sup>238</sup>U ages of 211 ± 1.2 Ma. This age is similar to the previously reported zircon LA-ICPMS U-Pb ages for the Zhashui plutons, which suggests that both the Zhashui plutons and Qinglingou granite porphyries formed during Late Triassic (Table 5). In addition, granitoids from Dongjiangkou, Zhashui, Shahewan and Caoping (Figure 2) also gave zircon LA-ICPMS U-Pb ages of 246–209 Ma [8–10,14], 234–214 Ma [9,12], 212–205 Ma [11,13] and 224–220 Ma [6,9], respectively. Hence, the Qinglingou granite porphyry in the area has an affinity with the Dongjiangkou, Zhashui, Shahewan, and Caoping plutons, and all of them were the products of the Late Triassic magmatic event. Although the precise metallogenic age of the Qinglingou gold deposit was not well constrained, it can be inferred that the

age of Au mineralization in the Qinglingou is later than that of the dikes according to the geological characteristics that the Au ore body occurs in the altered dikes. On the one hand, most scholars consider that the genesis of Carlin-type gold deposits is related to magmatism [55,56]. The granite porphyry from the Qinglingou deposit gave zircon LA-ICPMS U-Pb ages of  $211 \pm 1.2$  Ma. Meanwhile the Yangmugou ( $203.6 \pm 8.7$  Ma) Mo deposit was developed at a similar time in the Zhashui-Shanyang area (Table 4). It is suggested that the intrusive and metallogenic ages of Qinglingou gold deposit are consistent within the error range, which further reveals that there are Indosinian intrusive and metallogenic events in the Zhashui-Shanyang area of the South Qinling Belt.

### 5.2. Source of the Granitoid Stocks and Its Implications

The zircon Lu-Hf isotopic system has a high closure temperature, and the  $^{176}\text{Hf}/^{177}\text{Hf}$  values of zircon is less affected by the uncertainty of age. Therefore, zircon in situ Hf isotopic analysis can effectively reveal the magmatic evolution and the source area [57]. When a magmatic zircon initial  $\varepsilon_{\text{Hf}}(t)$  values are positive, it usually indicates that the source area is a depleted mantle or Cenozoic crust, while the negative  $\varepsilon_{\text{Hf}}(t)$  values indicate that the source area is ancient crust [58]. The heterogeneity of the zircon Hf isotope signature suggests that it has experienced a relatively significant process of crust-mantle magmatic mixing [59]. The range of  $\varepsilon_{\text{Hf}}(t)$  values is mainly concentrated between  $-0.08$ – $+1.98$ , close to 0, indicating that both a crustal source and lithospheric mantle components were involved in the magmatic source [60]. This result is supported by the Indosinian Shahewan, Caoping and Zhashui granites in this area, which also have homogeneous  $\varepsilon_{\text{Hf}}(t)$  values close to 0 (Figure 8). We argued that the depleted mantle material and the basic crustal material of the South Qinling basement may be the source material of the Indosinian granites in Zhashui-Shanyang area. Regionally, many studies have confirmed that the Shahewan, Caoping and Zhashui plutons from the Zhashui-Shanyang area are all of mixed crust-mantle magma origin. In summary, it can be reasonably inferred that the source of the Indosinian granites in the Zhashui-Shanyang area was derived from the thickened continental crust as a result of the underplating of mantle material.

Accompanying frequent tectonic movement, mineralization and magmatic activity, copper-gold deposits, closely related to Indosinian to Yanshanian magmatism, are widely developed in the Zhashui-Shanyang area. According to the relationship of deposits, some researchers have proposed that the disseminated gold deposits and porphyry–skarn copper-gold deposits in sedimentary rocks were formed in the same metallogenic system [61]. Importantly, Large et al. [62] have argued that the Carlin-type gold deposit was the distal product of the porphyry–skarn copper mineralization system. In terms of time, space, and genesis, the Yanshanian plutons in the district are related to the metallogenic ones of porphyry–skarn copper (molybdenum) deposits, such as Lengshuigou, Chigou, and Xiaohekou. As described above, previous studies have carried out an important magmatic-metallogenic event that resulted in the discovery of Cu-Mo-Au orebodies in the Late Jurassic–Early Cretaceous Chigou-Lengshuigou porphyries and their contact zones. The intensive Late Jurassic–Early Cretaceous magmatic activity also resulted in the emplacement of some granitoids in the form of small hypabyssal intrusions, such as the Xiaohekou, Lengshuigou, and Chigou granitic stocks in Zhashui-Shanyang area [63–66]. The Xiajiadian, Wangjiaping, and other Carlin gold deposits are 50 km away from the porphyry skarn Cu-Mo deposits, such as Chigou and Lengshuigou in Zhashui-Shanyang area [67–72]. These ages (150–145 Ma) of the Chigou and Lengshuigou Cu-Mo deposits in the Zhashui-Shanyang district are consistent with the dolomite Sm-Nd age of  $139.6 \pm 0.98$  Ma, which represents the age of Au mineralization in Xiajiadian Carlin-type Au deposit. The result is in correspondence with the views of previous studies [61,62].

Moreover, the Yangmugou porphyry molybdenum deposit is situated around 10 km west of the Qinglingou deposit and the molybdenite Re-Os is 203 Ma. This information indicates that the Xiajiadian, Wangjiaping, and Qinglingou deposits may belong to the distal Carlin-type gold deposit. The porphyry-skarn-Carlin-type deposits were distributed

in the Zhashui-Shanyang area. Similarly, we reasonably inferred that it is great potential for discovering Au deposits at the periphery of the porphyry-skarn Cu-Mo deposit in the studied area.

## 6. Conclusions

1. The Indosinian and Qinglingou granite porphyry have similar geochemical characteristics. The Indosinian granitoids are composed of quartz monzonite, granodiorite and granite series. Geochemical data show that the Qinglingou pluton is peraluminous and high-K calc-alkaline granite, similar to that of I-type granite. Isotopic characteristics of zircon Hf and regional geological evidence suggest that they resulted from the interplay of mantle- and crustal-derived magmas.
2. LA-ICPMS zircon U-Pb ages indicate that the Qinglingou granites were emplaced at  $213 \pm 2.1$  Ma. The close contact relationship between the Au ore body and the vein rock suggests that they may be the same products of the Late Triassic magmatic-metallogenic activity.
3. The comprehensive comparative analysis indicates that it is needed to strengthen the prospecting for the Carlin-type gold deposit in the periphery of the porphyry-skarn Cu-Mo deposits in the Zhashui-Shanyang area.

**Author Contributions:** Conceptualization, K.D. and X.Y.; methodology, K.D.; software, K.D. and Z.W.; validation, H.W. and X.Y.; formal analysis, K.D.; investigation, K.D.; K.L.; L.Z. and X.Y.; resources, K.D.; data curation, Z.W. and Y.L.; writing—original draft preparation, K.D.; writing—review and editing, K.D.; H.W. and X.Y.; visualization, K.D.; supervision, X.Y. and Y.C.; project administration, K.D.; funding acquisition, K.D. All authors have read and agreed to the published version of the manuscript.

**Funding:** This research was financially supported by the National Natural Science Foundation of China (41603040), Natural Science Basic Research Program of Shaanxi Province, China (2022JM-169), Scientific and Technological Innovation Team Project of Shaanxi Railway Institute (KJTD202001) and the Scientific Research Project of Shaanxi Railway Institute (KY2020-42).

**Acknowledgments:** We extend our thanks to the Mineralization and Dynamics Laboratory of Ministry of Land and Resources, Chang'an University, Xi'an, China; Laboratory of Beijing Kehui Testing Technology Co., Ltd., Beijing, China, and the Langfang Tuoxuan rock mine Testing Service Co., Ltd., China. We thank four anonymous reviewers for constructive comments on an earlier version of this paper.

**Conflicts of Interest:** The authors declare no conflict of interest.

## References

1. Zhang, G.W.; Zhang, B.R.; Yuan, X.C.; Xiao, Q.H. *Qinling Orogenic Belt and Continental Geodynamics*; Science Press: Beijing, China, 2001; pp. 1–855.
2. Liu, J.J.; Liu, C.H.; Wang, J.P.; Zhu, L.M.; Zhang, J.; Zhai, D.G.; Zhang, F.F. Classification and mineralization of the gold deposits in the western Qinling region, China. *Earth Sci. Front.* **2019**, *26*, 1–16.
3. Jin, X.Y.; Sui, J.X. Geochemistry of tourmaline from the Laodou gold deposit in the West Qinling Orogen, Central China: Implications for the ore-forming process. *Minerals* **2020**, *10*, 647. [[CrossRef](#)]
4. Goldfarb, R.J.; Mao, J.W.; Qiu, K.F.; Goryachev, N. The great Yanshanian metallogenic event of eastern Asia: Consequences from one hundred million years of plate margin geodynamics. *Gondwana Res.* **2021**, *100*, 223–250. [[CrossRef](#)]
5. Xie, G.Q.; Mao, J.W.; Wang, R.T.; Ren, T.; Li, J.B.; Dai, J.Z. Origin of late mesozoic granitoids in the newly discovered Zha-shan porphyry Cu district, south Qinling, central China, and implications for regional metallogeny. *J. Asian Earth Sci.* **2015**, *103*, 184–197. [[CrossRef](#)]
6. Jiang, Y.H.; Jin, G.D.; Liao, S.Y.; Zhou, Q.; Zhao, P. Geochemical and Sr-Nd-Hf isotopic constraints on the origin of Late Triassic granitoids from the Qinling orogen, central China: Implications for a continental arc to continent-continent collision. *Lithos* **2010**, *117*, 183–197. [[CrossRef](#)]
7. Wu, F.F. Study on Magmatic Rocks and Their Metallogenic Tectonic Environment in Shanyang- Zhashui Area, Middle Qinling Mountains. Ph.D. Thesis, Chinese Academy of Geological Sciences, Beijing, China, 2013.
8. Yang, K.; Liu, S.W.; Li, Q.G.; Wang, Z.Q.; Han, Y.G.; Wu, F.H.; Zhang, F. LA-ICP-MS zircon U-Pb geochronology and geological significance of Zhashui granitoids and Dongjiangkou granitoids from Qinling, central China. *J. Peking Univ. (Nat. Sci.)* **2009**, *45*, 841–847.

9. Liu, C.H.; Wu, C.L.; Gao, Y.H.; Lei, M.; Qin, H.P.; Li, M.Z. Zircon LA-ICP-MS U-Pb dating and Lu-Hf isotopic system of Dongjiangkou, Zhashui, and Liyuantang granitoid intrusions, South Qinling belt, central China. *Acta Petrol. Sin.* **2014**, *30*, 2402–2420.
10. Gong, H.J.; Zhu, L.F.; Sun, B.Y.; Li, Z.; Guo, B. Zircon U-Pb ages and Hf isotopic composition of the Dongjiangkou granitic and its mafic enclaves in the South Qinling terrain. *Acta Petrol. Sin.* **2009**, *25*, 3029–3042.
11. Gong, H.; Zhu, L.M.; Sun, B.Y.; Li, Z.; Guo, B. Zircon U-Pb ages and Hf isotope characteristics and their geological significance of the Shahewan, Caoping and Zhashui granitic plutons in the South Qinling orogen. *Acta Petrol. Sin.* **2009**, *25*, 248–264.
12. Hu, J.M.; Cui, J.T.; Meng, Q.R.; Zhao, C.Y. Zircon U-Pb age of Zhashui pluton in Qinling Mountains and its geological significance. *Geol. Rev.* **2004**, *50*, 323–329.
13. Wang, X.; Wang, T.; Jahn, B.M.; Hu, N.; Chen, W. Tectonic significance of Late Triassic post-collisional lamprophyre dykes from the Qinling Mountains (China). *Geol. Mag.* **2007**, *144*, 837–848. [[CrossRef](#)]
14. Qin, J.F. Genetic Mechanism and Deep Dynamic Background of Late Triassic granitoids in Qinling Orogenic Belt. Ph.D. Thesis, Northwest University, Xi'an, China, 2010.
15. Zhang, C.L.; Wang, X.X.; Wang, T.; Dai, M.N. Origin of shahewan granite intrusion in eastern Qinling: Evidences from zircon U-Pb dating and Hf isotopes. *J. Northwest Univ. (Nat. Sci. Ed.)* **2009**, *39*, 453–465.
16. Niu, B.G.; He, Z.J.; Ren, J.S.; Wang, J.; Deng, P. SHRIMP U-Pb ages of zircons from the intrusions in the western douling-xiaomaoling uplift and their geological significances. *Geol. Rev.* **2006**, *52*, 826–835.
17. Zheng, J.; Zhu, L.M.; Jiang, H.; Xiong, X.; Liu, K.; Zhao, D.H.; Li, Z.H.; Yang, Z.T.; Wang, H.; Peng, X. A comparisonal study on the indosinian and yanshanian granites of the Zhashui-Shanyang ore cluster district in the southern Qinling, China. *Bull. Mineral. Petrol. Geochem.* **2015**, *34*, 1155–1172.
18. Ren, T.; Wang, R.T.; Xie, G.Q.; Li, J.B.; Dai, J.Z.; Guo, Y.H. Geochemistry and rock\_ forming and ore\_ forming epochs of chigou cu porphyry deposit in shaanxi province, and their implications. *Miner. Depos.* **2014**, *33*, 807–820.
19. Zhou, B.; Wang, F.Y.; Sun, Y.; Sun, W.D.; Ding, X.; Hu, Y.H.; Ling, M.X. Geochemistry and tectonic affinity of Shahewan orogenic rapakivi from Qinling. *Acta Petrol. Sin.* **2008**, *24*, 1261–1272.
20. Zhu, L.M.; Zheng, J.; Xiong, X.; Jiang, H.; Liu, K.; Ding, L.L. Petrogeochemistry and mineralization potential of the Yuanzjijie intrusion in the Zhashui-Shanyang ore deposit cluster in southern Qinling. *Earth Sci. Front.* **2019**, *26*, 189–205.
21. Wu, F.F.; Wang, Z.Q.; Yan, Z.; Chen, L.; Xia, C.L.; Guo, Y.H.; Peng, Y.M. Geochemical characteristics, zircons U-Pb ages and Lu-Hf isotopic composition of the Yanshanian intermediate-acidic plutons in the Shanyang-Zhashui areas, Qinling Orogenic Belt. *Acta Petrol. Sin.* **2014**, *30*, 451–471.
22. Xie, G.Q.; Ren, T.; Li, J.; Wang, R.T.; Xia, C.L.; Guo, Y.H. Zircon U-Pb age and petrogenesis of ore-bearing granitoid for the Chigou Cu-Mo deposit from the zhashan basin, Shaanxi province. *Acta Petrol. Sin.* **2012**, *28*, 15–26.
23. Xiong, X.; Zhu, L.M.; Zhang, G.W.; Guo, A.L.; Zheng, J.; Jiang, H. Origin of the Xiaohekou skarn copper deposit and related granitoids in the Zha-Shan ore cluster area, South Qinling, China. *Ore Geol. Rev.* **2019**, *114*, 103143. [[CrossRef](#)]
24. Chen, L.; Wang, Z.Q.; Yan, Z.; Wu, F.F.; Ren, T.; Guo, Y.H. Metallogenesis of 150-140 Ma porphyry-skarn CuMoFe (Au) deposit in Shanyang-Zhashui ore concentration area, Qinling. *Acta Petrol. Sin.* **2014**, *30*, 415–436.
25. Meng, D.M.; Wang, R.T.; Liu, K.; Guo, Y.H.; Li, P.H. Geological characteristics and analysis of tectonic-magmatic-mineralization in chigou area of Shanyang county, Shaanxi province. *Northwest. Geol.* **2014**, *47*, 116–126.
26. Liu, K.; Wang, R.T.; Fan, Z.P.; Ren, T.; Li, J.B.; Zhao, L. Metallogenic age of xiajiadian gold deposit in the Zhashui-Shanyang ore concentration, qinling orogenic belt and its geological significance. *Miner. Depos.* **2019**, *38*, 1278–1296.
27. Liu, Y.S.; Hu, Z.C.; Zong, K.Q.; Gao, C.G.; Chen, H.H. Reappraisal and refinement of zircon U-Pb isotope and trace element analyses by LA-ICPMS. *Chin. Sci. Bull.* **2010**, *55*, 1535–1546. [[CrossRef](#)]
28. Ludwig, K.R. User's manual for a geochronological toolkit for Microsoft Excel (Isoplot/Ex version 3.0). 2003.
29. Yuan, H.L.; Gao, S.; Dai, M.N.; Zong, C.L.; Günther, D.; Fontaine, G.H. Simultaneous determinations of U-Pb age, Hf isotopes and trace element compositions of zircon by excimer laser-ablation quadrupole and multiple-collector ICP-MS. *Chem. Geol.* **2008**, *247*, 100–118. [[CrossRef](#)]
30. Middlemost, E.A. Naming materials in the magma/igneous rock mass system. *Earth-Sci. Rev.* **1994**, *37*, 215–224. [[CrossRef](#)]
31. Rickwood, P.C. Boundary lines within petrologic diagrams which use oxides of major and minor elements. *Lithos* **1989**, *22*, 247–263. [[CrossRef](#)]
32. Rollinson, H.R. *Using Geochemical Data: Evaluation, Presentation, Interpretation*; Longman Scientific and Technical: New York, NY, USA, 1993.
33. Sun, S.S.; McDonough, W.F. Chemical and isotopic systematics of oceanic basalts: Implications for mantle composition and processes. *Geol. Soc. Lond. Spec. Publ.* **1989**, *42*, 313–345. [[CrossRef](#)]
34. Stille, P.; Steiger, R.H. Hf isotope systematics in granitoids from the central and southern Alps. *Contrib. Mineral. Petrol.* **1991**, *107*, 273–278. [[CrossRef](#)]
35. Huang, Y.Q.; Qiu, K.F.; Yu, H.C.; Jin, D.G.; He, D.Y.; Xiao, C.H.; Wang, Y.X. Petrogenesis of ore-hosting porphyry in the Gelouang gold deposit, West Qinling and its geological implications. *Acta Petrol. Sin.* **2020**, *36*, 1567–1585.
36. Wang, B.; Hu, X.; Tang, L.; Li, J. Geochemistry, Zircon U-Pb Geochronology and Hf-O Isotopes of the Banzhusi Granite Porphyry from the Xiong'er shan Area, East Qinling Orogen, China: Implications for Petrogenesis and Geodynamics. *Minerals* **2019**, *9*, 538. [[CrossRef](#)]

37. Feng, J.Z.; Wang, D.B.; Wang, X.M.; Shao, S.C.; Ma, Z.G.; Zhang, X.G. Geology and metallogenesis of the Baguamiao giant gold deposit in Fengxian, Shaanxi province. *Acta Geol. Sin.* **2003**, *77*, 387–398.
38. Huang, J.; Wang, J.Y.; Wei, L.M. Geological characteristics and genesis of the Liba gold deposit, Gansu province. *Miner. Depos.* **2000**, *19*, 105–115.
39. Yang, G.S.; Chen, Y.W.; Hu, X.L.; Wang, J.X.; Yin, G.; Tang, Y.G. Geological-geochemical features and genesis of Dugou gold deposit of Li county, Gansu Province. *Northwest. Geol.* **2007**, *40*, 75–84.
40. Yang, S.S. *Study on Intermediate acid Magmatism and Gold Mineralization in Zhongchuan Area, West Qinling Mountains*; China University of Geosciences: Beijing, China, 2017.
41. Yu, C. *Study on Metallogenic Characteristics and Nonlinear Metallogenic Dynamics of Zhaishang Gold Deposit in West Qinling*; China University of Geosciences: Beijing, China, 2015.
42. Zhang, H.P. Ore controlling factors and prospecting criteria of No. 4 ore belt in Maquan gold deposit Gansu Province. *Gansu Geol.* **2009**, *18*, 41–45.
43. Qi, J.Z.; Yuan, S.S.; Li, L.; Sun, B.; Guo, J.H.; Li, Z.H.; Fan, Y.X.; Liu, W.; Gao, Q.B. Geological features and ore-controlling factors of the Yangshan superlarge gold deposit, Gansu province, China. *Geol. Rev.* **2003**, *49*, 85–92.
44. Zhang, J. *Study on Metallogenic Process and Mechanism of Baguamiao Super Large Gold Deposit in Fengtai Ore Cluster Area, Shaanxi Province*; Chinese Academy of Geological Sciences: Beijing, China, 2016.
45. Liu, X.L. *Geological and Geochemical Characteristics and Genesis of Chaima Gold Deposit in Fengxian County, Shaanxi Province*; China University of Geosciences: Beijing, China, 2014.
46. Wang, Y.T.; Li, X.; Wang, R.T.; Liu, X.L.; Hu, Q.Q.; Li, J.H.; Wang, C.G.; Wen, B.; Wen, S.W.; Wang, S.L. Evidence of Ar-Ar age for the metallogenic epoch of simaoling gold deposit in Fengxian-Taibai ore cluster of Shaanxi. *J. Earth Sci. Environ.* **2014**, *36*, 61–72.
47. Qiu, K.F.; Yu, H.C.; Deng, J.; McIntire, D.; Gou, Z.Y.; Geng, J.Z.; Goldfarb, R. The giant Zaozigou Au-Sb deposit in West Qinling, China: Magmatic-or metamorphic-hydrothermal origin. *Miner. Depos.* **2020**, *55*, 345–362. [[CrossRef](#)]
48. Wang, K.Y.; Yao, S.Z.; Yang, Y.C.; Dai, J.Z. Geological characteristics and origin of Manaoke fine-grained disseminated gold deposit in northwestern Sichuan province. *Miner. Depos.* **2004**, *23*, 494–501.
49. Zhang, X.J.; Zhang, J.; Jia, Y.S.; Zhou, Q.W. Geological and geochemical features of the Jinmuda gold deposit in north-western Sichuan province. *Geol. Explor.* **2002**, *38*, 28–32.
50. Zhao, L.Q.; Chen, X.; Zhou, H.; Li, X.M. Metallogenic age of Jinlongshan micro disseminated gold deposit in South Qinling Mountains. *Sci. Geol. Sin.* **2001**, *36*, 145–149.
51. Liu, Y.H.; Li, Z.; Zhou, S.; Han, Y.X.; Li, H.; Li, X.; Zhou, S.F. Geological characteristics, ore-forming ages and geological significance of Donggou-Jinlongshan gold deposit, south Qinling belt. *Earth Sci. Front.* **2016**, *23*, 81–93.
52. Chen, J. *Mesozoic Orogenic Gold Mineralization in East Qinling China*; University of Geosciences: Beijing, China, 2018.
53. Tang, K.F. *Temporal and Spatial Evolution, Genesis and Tectonic Setting of Gold Deposits in Xiongershan Area, Southern Margin of North China Craton*; China University of Geosciences: Wuhan, China, 2014.
54. He, X.Y. *Gold Molybdenum Metallogenic System in Xiongershan Waifangshan Ore Cluster Area*; China University of Geosciences: Beijing, China, 2017; pp. 1–202.
55. Cline, J.S.; Hofstra, A.H.; Muntean, J.L.; Tosdal, R.M.; Hickey, K.A. Carlin-type gold deposits in Nevada critical geologic characteristics and viable models. *Econ. Geol.* **2005**, 451–484. [[CrossRef](#)]
56. Muntean, J.L.; Cline, J.S.; Simon, A.C.; Longo, A.A. Magmatic-hydrothermal origin of Nevada’s Carlin-type gold deposits. *Nat. Geosci.* **2011**, *4*, 122–127. [[CrossRef](#)]
57. Griffin, W.L.; Pearson, J.; Belousova, E.; Jackson, S.V.; Van Achterbergh, E.; O’Reilly, S.Y.; Shee, S.R. The Hf isotope composition of cratonic mantle: LA-MC-ICPMS analysis of zircons megacrysts in kimberlites- Kimberlites and related rocks. *Geochim. Cosmochim. Acta* **2000**, *64*, 133–147. [[CrossRef](#)]
58. Wu, F.Y.; Li, X.H.; Zheng, Y.F.; Gao, S. Lu-Hf isotopic systematics and their applications in petrology. *Acta Petrol. Sin.* **2007**, *23*, 185–220.
59. Ding, K.; Liang, T.; Yang, X.Q.; Zhou, Y.; Feng, Y.G.; Li, K.; Teng, J.X.; Wang, R.T. Geochronology, genesis and tectonic significance of Dahongliutan pluton in West Kunlun orogenic belt. *J. Cent. South Univ.* **2019**, *26*, 3420–3435. [[CrossRef](#)]
60. Zheng, Y.F.; Chen, R.X.; Zhang, S.B.; Tang, J.; Zhao, Z.F.; Wu, Y.B. Zircon Lu-Hf isotope study of ultrahigh-pressure eclogite and granitic gneiss in the dabie orogen. *Acta Petrol. Sin.* **2007**, *23*, 317–330.
61. Sillitoe, R.H.; Bonham, H.F. Sediment-hosted gold deposits: Distal products of magmatic-hydrothermal systems. *Geology* **1990**, *18*, 157–161. [[CrossRef](#)]
62. Large, S.J.; Bakker, E.Y.; Weis, P.; Wälle, M.; Ressel, M.; Heinrich, C.A. Trace elements in fluid inclusions of sediment-hosted gold deposits indicate a magmatic-hydrothermal origin of the Carlin ore trend. *Geology* **2016**, *44*, 1015–1018. [[CrossRef](#)]
63. Wang, R.T.; Wang, X.Y.; Ren, T.; Li, J.B.; Meng, D.M.; Dai, J.Z. Study on exploration methods combination for porphyry- and skarn-type metal ore deposit in Zhashui-Shanyang concentration area. *Acta Petrol. Sin.* **2015**, *31*, 245–260.
64. Xie, G.Q.; Mao, J.W.; Wang, R.T.; Meng, D.M.; Sun, J.; Dai, J.Z.; Ren, T.; Li, J.B.; Zhao, H.J. Origin of the Lengshuigou porphyry-skarn Cu deposit in the Zha-Shan district, South Qinling, central China, and implications for differences between porphyry Cu and Mo deposits. *Miner. Depos.* **2017**, *52*, 621–639. [[CrossRef](#)]
65. Xiong, X.; Zhu, L.M.; Zhang, G.W.; Zheng, J.; Jiang, H. Insights into the skarn Cu mineralization processes of an intracontinental setting: A case study of the Xiaohekou deposit, Southern Qinling Orogen, China. *J. Geochem. Explor.* **2021**, *230*, 106862. [[CrossRef](#)]

66. Chen, L.; Yan, Z.; Wang, Z.Q.; Wang, K.M. Petrogenesis of early cretaceous dioritic dikes in the Shanyang-Zhashui area, south Qinling, central China: Evidence for partial melting of thickened lower continental crust. *J. Asian Earth Sci.* **2018**, *158*, 324–335. [[CrossRef](#)]
67. Wang, R.T.; Li, J.B.; Ren, T.; Yang, Z.H.; Mao, J.W.; Wang, T. Metallogenic conditions and prospecting potential of the Zhashui-Shanyang poly-metal ore cluster. *Geol. China* **2008**, *35*, 1291–1298.
68. Fang, W.X.; Liu, J.J. Dynamics of the late Paleozoic apart-pull basin and its relationship with mineralization of gold-silver-polymetallic-barite-siderite deposits in Zha-Shan-Shang, Shaanxi province. *Acta Sedimentol. Sin.* **2013**, *31*, 193–209.
69. Cao, D.H.; Zhu, L.M.; Li, Z.; Yang, D.M. Preliminary study on geological features and genesis of Wangjiagou gold deposit in Zhashui county, Shanxi province. *Geol. Explor.* **2009**, *45*, 23–29.
70. Ding, K.; Wang, R.T.; Liu, K.; Wang, Z.H.; Shen, X.M. Sulfide trace elements and sulfur isotope geochemistry of the Longtougou gold deposit, Zhashui-Shanyang ore district, South Qinling. Characteristics. *Geol. Explor.* **2021**, *57*, 969–980.
71. Qiu, K.F.; Goldfarb, R.J.; Deng, J.; Yu, H.C.; Gou, Z.Y.; Ding, Z.J.; Wang, Z.K.; Li, D.P. Gold deposits of the Jiaodong Peninsula, eastern China. *SEG Spec. Publ.* **2020**, *23*, 753–773.
72. Huang, Y.Q.; Wu, M.Q.; Germain, B.; Yu, H.C.; Qiao, B.X.; Zhao, Z.G.; Qiu, K.F. Geodynamic setting and ore formation of the Younisayai thorium deposit in the Altyn orogenic belt, NW China. *Ore Geol. Rev.* **2021**, *140*, 104552. [[CrossRef](#)]